HHS Public Access

Author manuscript

Biomaterials. Author manuscript; available in PMC 2018 October 25.

Published in final edited form as:

Biomaterials. 2018 October ; 181: 347–359. doi:10.1016/j.biomaterials.2018.07.015.

Optimal electrical stimulation boosts stem cell therapy in nerve regeneration

Jian Du[a], **Gehua Zhen**[b], **Huanwen Chen**[a], **Shuming Zhang**[c,d], **Liming Qing**[a], **Xiuli Yang**[a], **Gabsang Lee**[e,f], **Hai-Quan Mao**[c,d], and **Xiaofeng Jia**[a,c,g,h,i,*]

[a]Department of Neurosurgery, University of Maryland School of Medicine, Baltimore, MD, 21201, USA

[b]Department of Orthopaedics, Johns Hopkins University School of Medicine, Baltimore, MD, 21205, USA

[c]Department of Biomedical Engineering, Johns Hopkins University School of Medicine, Baltimore, MD, 21205, USA

[d]Department of Materials Science and Engineering, Johns Hopkins University School of Medicine, Baltimore, MD, 21205, USA

[e]Department of Neurology, Johns Hopkins University School of Medicine, Baltimore, MD, 21205, USA

[f]Department of Neuroscience, Johns Hopkins University School of Medicine, Baltimore, MD, 21205, USA

[g]Department of Orthopedics, University of Maryland School of Medicine, Baltimore, MD, 21201, USA

[h]Department of Anatomy Neurobiology, University of Maryland School of Medicine, Baltimore, MD, 21201, USA

[i]Department of Anesthesiology and Critical Care Medicine, Johns Hopkins University School of Medicine, Baltimore, MD, 21205, USA

Abstract

Peripheral nerve injuries often lead to incomplete recovery and contribute to significant disability to approximately 360,000 people in the USA each year. Stem cell therapy holds significant promise for peripheral nerve regeneration, but maintenance of stem cell viability and differentiation potential in vivo are still major obstacles for translation. Using a made-in-house 96-

*Corresponding author. 685 West Baltimore Street, MSTF Building 823, Baltimore, MD, 21201, USA, xjia@som.umaryland.edu (X. Jia).

Conflicts of interest

The authors state no conflict of interest.

Data availability

The raw/processed data required to reproduce these findings cannot be shared at this time as the data also forms part of an ongoing study.

Appendix A. Supplementary data

Supplementary data related to this article can be found at https://doi.org/10.1016/j.biomaterials.2018.07.015.

well vertical electrical stimulation (ES) platform, we investigated the effects of different stimulating pulse frequency, duration and field direction on human neural crest stem cell (NCSC) differentiation. We observed dendritic morphology with enhanced neuronal differentiation for NCSCs cultured on cathodes subject to 20 Hz, 100μs pulse at a potential gradient of 200 mV/mm. We further evaluated the effect of a novel cell-based therapy featuring optimized pulsatile ES of NCSCs for in vivo transplantation following peripheral nerve regeneration. 15 mm critical-sized sciatic nerve injuries were generated with subsequent surgical repair in sixty athymic nude rats. Injured animals were randomly assigned into five groups (N = 12 per group): blank control, ES, NCSC, NCSC + ES, and autologous nerve graft. Optimized ES was applied immediately after surgical repair for 1 h in ES and NCSC + ES groups. Recovery was assessed by behavioral (CatWalk gait analysis), wet muscle-mass, histomorphometric, and immunohistochemical analyses at either 6 or 12 weeks after surgery (N = 6 per group). Gastrocnemius muscle wet mass measurements in ES + NCSC group were comparable to autologous nerve transplantation and significantly higher than other groups ($p < 0.05$). Quantitative histomorphometric analysis and catwalk gait analysis showed similar improvements by ES on NCSCs ($p < 0.05$). A higher number of viable NCSCs was shown via immunochemical analysis, with higher Schwann cell (SC) differentiation in the NCSC + ES group compared to the NCSC group ($p < 0.05$). Overall, ES on NCSC transplantation significantly enhanced nerve regeneration after injury and repair, and was comparable to autograft treatment. Thus, ES can be a potent alternative to biochemical and physical cues for modulating stem cell survival and differentiation. This novel cell-based intervention presents an effective and safe approach for improved outcomes after peripheral nerve repair.

Keywords

Pluripotent stem cells; Human neural crest stem cell; Electrical stimulation; Peripheral nerve injury; Nerve regeneration

1. Introduction

Peripheral nerve injury (PNI) is a common global clinical problem, affecting 20 million Americans, and costing over $150 billion of annual spending [1]. Despite great improvements in microsurgical techniques, recovery is often incomplete, resulting in neuropathic pain and poor function [1]. In particular, critical-sized nerve gaps present challenges to peripheral nerve repair as they portend poorer recovery. Currently, autograft implantation is considered the standard clinical treatment, however, limited availability of donor tissue, donor site morbidity, and size mismatch between donor and recipient nerves limit the application of this technique [2,3]. Thus, better repair strategies for peripheral nerve gap injuries are of great interest.

Various strategies for improving nerve repair have been proposed in basic, pre-clinical and clinical trials [4–6]. Stem cell transplantation therapy has emerged as a particularly promising strategy to improve outcomes in pre-clinical models [7–9]. More specifically, neural crest stem cells (NCSCs) increase the rate of early axon regeneration and enhance neuronal survival [8], making them an appealing choice for nerve regeneration. In vivo pre-

clinical studies have shown that NCSCs promote nerve regeneration by differentiating into Schwann-like cells, facilitating the myelination of axons, and exerting neuroprotective effects to guide the growth direction of regenerated axons [8]. However, the low success rate of self-renewal, limited survival, and poor differentiation of transplanted stem cells limit the potential for clinical translation [10].

Electrical fields can have profound impacts on cell migration, proliferation, and axonal outgrowth via modulations in ion channel distribution [11], and electrical stimulation (ES) can enhance stem cell differentiation towards electrically active cell types such as cells in the nervous system. ES significantly increases the proliferation and differentiation of fetal neural stem cells into neuronal cells [12], and strongly promotes cell differentiation of human neural stem cells [13] and embryonic stem cells [14]. Furthermore, *in vivo* studies also revealed that ES promotes the release of neurotrophic factors [15], which maintain survival and proliferation of stem cells after nerve injury and facilitate stem cell differentiation into Schwann Cell-like cells [10,16]. ES has also been reported to directly promote axon regeneration in pre-clinical [17] and clinical [18] settings by mimicking action potentials from the central nervous system, which increases local synthesis of the major protein in myelin sheaths, therefore stimulating myelin induction [19]. Despite convincing evidence that ES impacts NCSC differentiation and axon regeneration, the optimal conditions of ES and the overall effect of ES on stem cell-based nerve regeneration therapy remains largely unknown.

The main objective of this study is to develop a novel cell-based peripheral nerve repair strategy using ES to enhance NCSC transplantation. Traditional devices for *in vitro* ES testing may suffice for single-waveform stimulations, however, they generally do not allow for simultaneous investigations of multiple stimulation parameters. The capability to simultaneously reproduce multiple complex simulations in vitro is critical for investigating the role of each stimulation while limiting extrinsic variance between experiments to clearly delineate the individual or synergistic effects on the development, function, differentiation or regeneration of the cells [20]. To this end, we designed a 96-well ES platform that accommodates simultaneous application of multiple ES parameters such as field polarity, electrical potential, pulsing frequency, and stimulation duration for inducing NCSC differentiation, identified optimal conditions, and applied these optimal variables *in vivo* in a critically-sized (15 mm) rat sciatic nerve injury model. NCSC differentiation, Schwann cell proliferation, neurite regrowth, axon myelination, nerve conductivity, muscle re-innervation, and functional recovery were evaluated over 12 weeks and compared across 5 gap repair strategies: empty polycaprolactone nanofiber nerve conduit without ES (control), empty conduit with ES, NCSC filled conduit without ES, and NCSC filled conduit with ES, autograft transplantation. Our combined intervention of NCSC transplantation with ES synergistically boosted regeneration in critical-sized sciatic nerve defects. The recovery outcomes were comparable to those of autograft implantation.

2. Materials and methods

2.1. Electrical stimulation platform

Our electrostimulation study was performed with a built-in-house platform that generates a vertical electric field with electrodes placed in a top-bottom configuration (illustrated in Fig. 1A&B). The vertical configuration contrasts with conventional horizontal electrical potential gradients [21] by its ability to stimulate a larger area of cells and separate the effects of galvanic migration resulting from cell differentiation. The top electrodes (99.999% pure gold wires, Surepure, Chemetals, Florham Park, NJ, USA) are connected to a printed circuit board, and the bottom electrodes are made by depositing chromium and gold onto glass via e-beam vapor deposition. The gold nature of the two electrodes prevents electrochemical reactions with the sample solution during stimulation. The deposition process for the bottom electrode involved cleaning the glass with Piranha solution for 10 min, rinsing with deionized water, and then air-drying. Then, via patterned mask, an electrode array was created by vapor depositing a 3-nm chromium layer and a 12-nm gold layer onto the glass surface. This design provides a stable coating on the glass and leaves enough optical transparency for light transmission microscopy imaging. The cell walls were made with polydimethylsiloxane (PDMS). We mixed Sylgard 184 silicone elastomer base and curing agent (10:1) in a 90° C metal mold for one hour. Then, we fixed the bottom electrode plate with a thin layer of PDMS. We used silver paste to create the electrical contact between the gold substrate and the ground electrode.

2.2. Electrical stimulation of NCSC in vitro

Human NCSCs (hNCSCs) were derived from embryonic stem cells (ESCs, H9 line from WiCell, Madison, WI) according to protocols reported by Lee [22], and expanded for 5 days in neurobasal medium supplemented with B27 and 20 ng/ml of FGF2 and EGF. We designed an electrostimulator in 96-well culture plate format that permits easy modulation of multiple parameters, and used this custom-designed stimulator to deliver adjustable electrical outputs to cells in individual wells, thus increasing the throughput of the assay (Fig. 1). Prior to electrostimulation, the custom-made culture plates were coated with 15 mg/ml polyornithine (PO) and 1 mg/ml fibronectin/laminin (FN/Lam), and hNCSCs were seeded at a density of 1, 5, and 10×10^4 cells/cm^2 on the coated gold substrate. After 2 days of culture, electrostimulations were applied to cells.

Stimulations with different amplitudes/potential gradients, frequencies, and durations were applied. Comparing with continuous stimulation, pulsatile stimulation could minimize heat generation and electrolyte depletion as well as reduce shear stress, thus prevent cell damage and enhance signal transport [23]. Both bottom-grounded and top-grounded configurations were first tested in this study. Compared with continuous stimulation, pulsatile stimulation minimizes heat generation and electrolyte depletion at the electrode-medium interface. First, we identified the optimal potential and duration of ES based on the previous studies [15,23,24], and found that 200 mV/mm potential and 100 μs of duration were the optimal conditions. Then, we applied these conditions to cells after 24 h of culture for 1, 3 or 8 h of pulsatile electrostimulations with different frequencies (2, 20 (which is the physiologically relevant frequency of hindlimb motoneuron discharge [25]), and 100 Hz) and repeated these

ES sessions for 3 [23] or 8 [26] consecutive days (Supplementary Table 1). For each condition, cells were seeded in quadruplets. NCSCs survival and SC differentiation were evaluated by co-labeling with standard markers for neurons (ßIII-tubulin) and SCs (S100b). Unless stated otherwise, all cell culture media and supplies were purchased from Life Technologies (Grand Island, NY, USA).

2.3. Sciatic nerve transection and repair

All animals were maintained in accordance with NIH guidelines for the humane care of animals and experimental protocols were reviewed and approved by the IACUC of University of Maryland School of Medicine. Sixty athymic nude rats (200e250 g) were randomly divided into five groups (12 rats in each) based on the type of nerve repair: (A) control conduit filled with PBS (CTL), (B) conduit with ES applied (ES), (C) conduit filled with NCSCs (NCSC), (D) conduit filled with NCSCs with ES applied (NCSC + ES), and (E) autologous nerve graft (Autograft). The optimal parameters for ES were determined during the in vitro portion of this study and used for the *in vivo* portion. The rats were anesthetized by inhalation of isoflurane. The right leg was sterilely prepared and the sciatic nerve exposed. A 15 mm segment of the right sciatic nerve of each animal was transected 0.5 cm proximal to the bifurcation of the sciatic nerve, and then either a polycaprolactone nanofiber nerve conduit (an average inner diameter the nerve guides are of (1.5 ± 0.2) mm and wall thickness of (83.2 ± 2.9) μm), which has been developed and validated [27], or autograft was sewn in while maintaining an inter-stump distance of 15 mm. Autografts were obtained by reverse implantation of the 15 mm segment of resected sciatic nerve. Prior to implantation, the nerve conduits were sterilized via ethylene oxide treatment. Nerve conduits with 17 mm in length were retained in place using four 9/0 epineurial sutures with the proximal and distal nerve stumps inserted 1 mm into the conduit. For the groups with NCSCs, Collagen I Rat Tail (Life Technologies, NY) was thawed inside an ice bath overnight until it returned to the liquid state. An NCSC medium loaded hydrogel was prepared by mixing the liquidized hydrogel with 2×10^6 NCSCs suspended in a 15 μl mixture of growth medium in 1:1 proportion inside an ice bath, and injected into the conduit. For the groups with ES, stimulation was performed using parameters determined from the in vitro portion of this study. Wounds were then closed in layers, and animals in each group were allowed to recover. The animals had free access to food and water before and after the experiments, and were housed under temperature controlled conditions at 21 ± 1 °C with a normal 12/12 h light/dark cycle. At either the 6 or 12 weeks time period, half of the rats (6 rats in each group) were euthanized. Transverse cryostat sections (10 μm thick) were prepared from the middle parts of the conduits for immunohistochemical staining and histomorphometric analysis.

2.4. Intrafascicular ES of axotomized and repaired nerves

In the stimulation groups, after nerve repair, 2 modified intrafascicular electrodes were implanted in both sides of the sciatic nerve stump 0.5 cm from the suture site, as we previously described [28–31]. The insulated electrodes were led to a stimulator (Grass S48 Square Pulse stimulator, Astro-Med Inc, West Warwick, RI). ES was applied between the cathode placed at the distal stump and the anode at the proximal stump. The nerve and their regenerating axons were subject to 1-h continuous ES immediately after repair of the nerve,

with supramaximal pulses (100 μsec; 3 V) delivered in a continuous 20 Hz train based on the in vitro study. The intrafascicular electrodes were removed after ES and the incision was closed in layers. The illustration of animal experimental design and procedures was shown in Fig. 2.

2.5. Immunohistochemistry

At the 12 week time point, regenerated nerves were washed with PBS then blocked in 5% normal goat serum in 0.2% Triton-XPBS for 60 min, and immunostained using rabbit anti-Neurofilament 200 (N 200, 1:1000, Sigma), mouse NGFR p75 antibody (p75, 1:300, Santa Cruz Biotechnology), Chicken BIIITubulin (1:1000, Millipore), rabbit anti-S100 antibody (1:400, Dako), or mouse anti-Human HuNu (1:200, EMD Millipore) to detect axons, SCs, and hNCSC cells, followed by visualization with Alexa-conjugated secondary antibodies. Primary and secondary antibodies were incubated overnight at 4° C and at room temperature for 60 min, respectively. The stained slides were mounted in Prolong Gold with DAPI (Invitrogen, Carlsbad, CA), and subsequently imaged by fluorescent Nikon Ti-E inverted microscope (Nikon, Kobe, Japan). Appropriate controls included negative controls where primary antibodies were omitted and positive controls of tissue sections known to express the antigen under study. Immunostaining intensity was analyzed using ImageJ. The total corrected cellular fluorescence (TCCF) was calculated using the formula: TCCF ¼ integrated density e (area of selected cell × mean fluorescence of background readings). The TCCF was then compared against the mean TCCF of neighboring interphase cells in the same field of view, with results presented as fold increase over interphase levels [32]. The number of HuNu positive cells and the proportion of HuNu/S-100 double-labeled cells to HuNu positive cells per slide were analyzed by ImageJ software (National Institutes of Health, Bethesda, MD) [33]. 6 animals per group (30 mm thickness, 6e8 sections per animal) were included in this analysis.

2.6. Histomorphometric analysis

Upon retrieval of the nerve conduits at 6 or 12 weeks postimplantation, nerve cross-sections at 8–10 mm from the proximal end were processed for toluidine blue staining. The specimens were fixed in 4 wt % paraformaldehyde overnight, and then post-fixed with 2% of osmium tetroxide for 2 h and dehydrated prior to mounting in embedding resin. For semithin sections, 0.5 μm thick specimens were sectioned on an Ultracut E microtome and stained with 1% toluidine blue for light microscopy (Nikon Ti-E inverted microscope, Nikon, Kobe, Japan). Four cross-sections were cut from each nerve, and the whole sciatic nerves were imaged. A randomly chosen set of images representing at least 30% of the cross-sectional nerve area were acquired at 100 × from mid parts of the tube or graft. The histomorphology of toluidine blue stained semi-thin sections after 6 and 12 weeks was blindly and quantitatively assessed. Myelinated fibers were counted by using ImageJ software (National Institutes of Health, Bethesda, MD). Density is calculated as the number of myelinated axons per 10,000 μm^2. The lengths of the outer and inner margins of the myelin sheath were measured to determine the fiber diameter (FD) and axon diameter (AD), and the myelin thickness = FD-AD [34].

2.7. Electrophysiological study

Electrophysiological recording was conducted for all animals at baseline, then at 6 or12 weeks prior to euthanasia, with a Tucker-Davis Technologies system (TDT, Alachua, FL) via a preamplifier. A ground electrode was placed in the tail of the subject. With stimulation intensity of the sciatic nerve (500 μA or 1 mA, 100 μs pulse duration, and a stimulation frequency of 0.5 Hz) via the proximal needle electrodes, compound motor action potential (CMAP) recordings from the distal nerve, and motor evoked potential (MEP) from the tibialis anterior muscle were recorded. Each recording lasted for 1 min, followed by 2 min relaxation periods, and repeated four times at each stimulation intensity. Peak-to-peak amplitude and latency of the largest peak in CMAP and M wave in MEP were analyzed offline in MATLAB. Peaks were detected with a threshold, which was set to two or three times the standard deviation above the mean of the signal, based on the signal-to-noise ratio [33,35]. Peaks below this threshold were considered noise.

2.8. Wet weight of gastrocnemius muscle

After harvesting the nerve for the histological analysis, gastrocnemius muscles were dissected and harvested carefully from both injured and uninjured sides for weighing using an electronic balance (Mettler AE 160, USA). The muscle weight absolute value is subject to differences in body mass between group members. We chose to use the Gastrocnemius Muscle Index (GMI) to compare the groups for the degree of muscle-mass recovery following the atrophy caused by the transient denervation [36]. The GMI was blindly assessed by dividing the gastrocnemius muscle mass on the experimental side by that on the control side. We performed H&E staining to investigate the morphological changes in the gastrocnemius muscle.

2.9. Behavioral assessment

We have described the methodology of CatWalk (Noldus Information Technology, The Netherlands) before [6,37,38]. Briefly, one week prior to surgery, animals were trained daily on a CatWalk runway until they were able to make consecutive uninterrupted runs. Animals were placed on the right side of a runway and motivated to cross the runway toward the left end. Six compliant trials were recorded by a computer running Catwalk XT 10.5 Software (Noldus) for each animal per time point, and five animals for each group. All trials marked by the software as compliant were reviewed manually: if the animal stopped or turned in mid-run the trials were excluded in the analysis. Thus a minimum of three validated runs were available each time point per animal. The stand time and duty cycle parameters, which show the time spent per step and percentage of time per step cycle spent bearing weight for each paw respectively, were collected and blindly assessed. Animals performed runs at the 2, 6, and 12 week time points. In order to prevent the confounding effects of walking speed and animal weight, the non-impaired contralateral hind paws were used for control comparison, and results are reported as Right to Left (R/L) ratios. All data were normalized by the control legs and presented in percentage.

2.10. Statistical analysis

Data were expressed as the mean ± standard error of the mean (SEM). Statistical significance was evaluated using univariate ANOVAs followed by post hoc paired comparisons using the Least-Significant Difference (LSD) or Student-Newman-Keuls tests when appropriate. Repeated Measures ANOVA Analysis was used to evaluate CatWalk Data followed by LSD post hoc analysis. Fisher's Exact test was used when appropriate. Values of $P < 0.05$ were considered significant. All statistical tests were carried out with statistical software SPSS 20.0 (IBM/SPSS Inc., Chicago, IL, USA).

3. Results

3.1. Optimal ES conditions for NCSC survival and differentiation in vitro

A custom made 96-well ES platform was fabricated in-house (Fig. 1A &B). Our made-in-house device features a circuit board integrated with a 96 well array, and is designed to serve as a high throughput stimulation platform where multiple stimulations (up to 96 conditions) can be applied simultaneously in the same study. This cell stimulation platform demonstrates the use of various modes of ES in guiding cellular behavior, and subsequently enables to study on physiologically-relevant stimulation signals.

To identify optimal ES conditions for NCSC survival and differentiation, we first explored the optimal density of NCSC cell seeding in this device, as cell-cell contact and communication significantly impact cell differentiation. At a lower density of 1×10^4 cells/cm^2, cells barely differentiated. At a higher density of 10×10^4 cells/cm^2, cells showed too much confluence after 8 days, and we were unable to observe cell differentiation. The cell density study showed that a seeding density of 5×10^4 cells/cm^2 was optimal for 8 days of stimulation. Therefore, 5×10^4 cells/cm^2 seeding density was used for subsequent tests.

Next, we tested the effects of polarity on NCSC differentiation and the optimal electrical potential gradient. NCSCs were stimulated with 50-ms pulses of 0 (control), 75, 150, and 200 mV/mm electrical potential gradient at 1 Hz for 24 h with two different configurations: cells cultured on the cathode (bottom electrode was grounded, referred to as Bg) and cells cultured on the anode (top electrode was grounded, referred to as Tg). We found that NCSCs cultured on the cathode with 150 mV/mm (Bg150) and 200 mV/ mm (Bg200) potential generated substantially higher numbers of neurite-like long processes comparing with the flat monolayer morphology for cells stimulated with lower potential (Bg75) and in the control group (Fig. 1C). Interestingly, cells stimulated with the same potential gradients but in reverse polarity (Tg) did not show any significant change in their morphology. Immunohistochemistry analysis further showed no SC differentiation at 3 days in all cases when cells were cultured on the anode (Tg configuration). Cellular morphological change and differentiation were dependent on these stimulation parameters and strongly dependent on the polarity of electrostimulation. Nonetheless, cells stimulated at Bg200 configuration showed visible signs of apoptosis when they were stimulated for more than 24 h. With stimulation periods of one hour per day, preferential differentiation occurred on cathodes rather than the anodes. Given these results, all subsequent experiments were performed with the Bg configuration at 200 mV/mm and one hour per day.

We then identified the optimal frequency and duration of stimulation. With one hour per day ES, we found no morphological difference in either 3 or 8 days. At day 3, the fluorescence micrographs of NCSCs were positive for βIIITubulin at all conditions (Fig. 3A: control, 2, 20 and 100 Hz). However, significant expression of S100 was only observed in the lower pulse frequency of 2 and 20 Hz (Fig. 3C&D). In addition, despite a brighter ßIII-Tubulin expression, cells likely underwent apoptosis with 100 Hz stimulation as indicated by rounded and shrunken cell morphology (Fig. 3B). 20 Hz induced SC differentiation with the higher fluorescence intensity of S100, and mature spindle-like SCs were best observed after ES with 200 mV/mm, 20hz, 100 μs (Fig. 3D). Since one-hour brief stimulation after a surgical repair has been shown to significantly accelerate axon regeneration [39,40], for better clinical translation, optimal ES parameters of 200 mV/mm, 20hz, and 100μs were applied continuously for one hour in our *in vivo* study immediately after repair. As electrical polarity significantly impacted NCSC survival and differentiation *in vitro* as we explored above, we used a direct current (DC) circuit for *in vivo stimulation*, with the cathode placed at the distal nerve stump and the anode at the proximal nerve stump.

3.2. ES promoted NCSC differentiation and proliferation *in vivo*

Immunofluorescence staining of cross sections from the middle portion of the conduit is shown in Fig. 4 and Supplementary Figure 1. We found no content in the conduit for the control (CTL) group (data not shown) and only a few cells in the ES group at both 6 and 12 weeks. At 6 weeks, Tubulin immunostaining for axons indicated that axons regenerated across the middle of the defect, and SCs are present within regenerated nerves in the NCSC and NCSC + ES groups as identified by S100 staining. In the autograft group, SCs colocalized closely with the regenerated axons and were wrapped around regenerated axons, indicating that SCs not only migrated and survived in this group but also functionally ensheathed regenerated axons (Supplementary Figure 1A). After 12 weeks, the number of axons with positive staining of S100 and Tubulin in NCSC and NCSC + ES groups were increased and became more uniform and denser, showing results comparable to the autograft group (Supplementary Figure 1B). The positive stained areas of N 200 and p75 in the NCSC + ES and autograft groups (Fig. 4A&B) were clearly higher than the ES and NCSC groups, with more than a 6-fold increase for N200 intensity (autograft:30.23 ± 2.92 and NCSC + ES: 25.42 ± 2.24 vs. NCSC: 5.50 ± 0.85 and ES: 4.56 ± 0.51, $p < 0.01$) and a 2-fold increase for p75 intensity (autograft: 8.29 ± 1.03 and NCSC + ES: 9.40 ± 0.37, vs. NCSC: 4.78 ± 0.92 and ES: 5.5 ± 0.85, $p < 0.05$) at 12 weeks.

HuNu (human nuclear antigen) positive cells were observed within a segment of the sciatic nerve in both the NCSC and NCSC + ES groups after 12 weeks (Fig. 5), which demonstrated that hNCSCs (HuNu positive) were able to be observed up to 12 weeks post-transplantation. In the NCSC + ES group, HuNu positive cell count was two-folds greater compared to the NCSC only group (NCSC + ES vs. NCSC, 42.67 ± 7.51 vs. 22.50 ± 2.57, $p < 0.05$, Fig. 5B). Double staining of HuNu and S-100 was evident, indicating that hNCSCs differentiation into Schwann-like cells (arrows in Fig. 5C). The NCSC þ ES group showed an increase in colocalization of HuNu and S100 signals (NCSC þ ES vs. NCSC, 13 ± 1.60 vs. 4.42 ± 0.57, $p < 0.001$, Fig. 5D). As the ES and autograft groups did not receive human NCSC transplantation, HuNu þ cells do not exist in the nerve specimen after regeneration.

Overall, these results indicate that hNCSCs are able to differentiate into peripheral nerve support cells, and that ES significantly promotes hNCSC differentiation into SCs *in vivo*.

3.3. Combined ES and NCSC therapy promoted axon regeneration and myelination

CTL and ES groups' nerve samples showed sparse and small patches at both 6 weeks (Fig. 6a and b, respectively) and 12 weeks (Fig. 6f and g, respectively), indicating unsuccessful regeneration in the presence of a critical-sized gap (15 mm). In the NCSC group (Fig. 6c and h), a larger number of myelinated axons was observed compared to the CTL and ES only groups. The NCSC + ES group (Fig. 6d and i) showed a comparable distribution profile to the autograft group (Fig. 6e and j). The temporal comparison showed an increased number of regenerating axons from 6 to 12 weeks for all groups. In contrast, axon diameter only marginally increased from 6 to 12 weeks.

3.3.1. Density—Overall across all time points, there was no significant difference existed between the NCSC + ES group and the autograft group ($p > 0.05$) (Fig. 6B). The NCSC + ES group showed significantly higher density compared with the ES and CTL groups (both $p < 0.001$). The Autograft group has significantly higher myelinated axon density than the NCSC, ES, and CTL groups ($p = 0.027$, $p < 0.001$, $p < 0.001$, respectively), and the NCSC group showed significantly higher density than the ES and CTL groups ($p = 0.034$, $p = 0.017$, respectively).

At 6 weeks, there was no significant difference between the NCSC + ES group and the autograft group ($p > 0.05$). The NCSC + ES group (25.75 ± 3.89) showed significantly higher density than the NCSC, ES, and CTL groups (10.71 ± 1.15, $p = 0.026$; 5.14 ± 2.98, $p = 0.007$; 3.60 ± 1.31, $p = 0.005$; respectively). The Autograft group (25.00 ± 6.26) also showed significantly higher values than the NCSC, ES, and CTL groups ($p = 0.044$, $p = 0.012$, $p = 0.009$, respectively). At 12 weeks, there was again no significant difference between the NCSC + ES group and the autograft group ($p > 0.05$). The NCSC + ES group (45.13 ± 7.79) has significantly higher myelinated axon density than the ES and CTL groups (15.04 ± 4.82, $p = 0.014$; 11.11 ± 2.72, $p = 0.006$; respectively), and the Autograft group (46.94 ± 6.13) also has significantly greater values than the ES and CTL groups ($p = 0.011$, p ¼ 0.006, respectively). The NCSC group (37.52 ± 6.06) showed significantly greater density than the CTL group ($p = 0.036$).

3.3.2. Diameter—By comparing the aggregate data from 6 to 12 weeks, the NCSC + ES group showed significantly larger axon diameter than the Autograft, NCSC, ES, and CTL groups ($p = 0.001$, $p = 0.001$, $p < 0.001$, $p < 0.001$, respectively) (Fig. 6C). The Autograft group also showed significantly larger diameter than the ES group ($p = 0.044$). All other comparisons showed no significant differences ($p > 0.05$).

At 6 weeks, the NCSC + ES group (4.90 ± 0.08 μm) showed significantly larger diameter than the Autograft, NCSC, ES, and CTL groups (4.51 ± 0.04 μm, $p = 0.005$; 4.65 ± 0.02 μm, $p = 0.035$; 4.55 ± 0.11 μm, $p = 0.008$; 4.66 ± 0.01 μm, $p = 0.040$; respectively). There was no significant difference between the Autograft group with any other group. At 12 weeks, the NCSC + ES group (4.99 ± 0.07 μm) showed significantly larger diameter than the NCSC, ES, and CTL groups (4.74 ± 0.05 μm, $p = 0.011$; 4.61 ± 0.06 μm, $p = 0.001$; 4.53

± 0.04 μm, $p < 0.001$; respectively). The Autograft group (4.85 ± 0.02 μm) also showed significantly larger diameter than the ES and CTL groups ($p = 0.014$, $p = 0.003$, respectively), and the NCSC group showed significance improvement compared with the CTL group ($p = 0.037$).

3.3.3. Percentage of total area occupied by myelinated axons—Overall across all time points, the NCSC + ES group showed significantly larger area than the NCSC, ES and CTL groups ($p = 0.005$, $p < 0.001$, $p < 0.001$, respectively) (Fig. 6D). The Autograft group also showed significantly larger area than the NCSC, ES, and CTL groups ($p = 0.012$, $p < 0.001$, $p < 0.001$, respectively), and the NCSC group showed significantly larger area than the ES and CTL groups ($p = 0.011$, $p = 0.002$, respectively).

At 6 weeks, the NCSC + ES group (7.48 ± 0.54%) showed significantly larger area than the Autograft, NCSC, ES, and CTL groups (4.86 ± 1.06%, $p = 0.020$; 2.73 ± 0.53%, $p = 0.001$; 0.93 ± 0.48%, $p < 0.001$; 0.75 ± 0.05%, $p < 0.001$; respectively). The Autograft group also showed significantly larger area than the ES and CTL groups ($p = 0.005$, $p = 0.004$, respectively). At 12 weeks, the NCSC group (10.32 ± 1.51%) showed significantly larger area than the ES and CTL groups (4.10 ± 1.40%, $p = 0.008$; 2.18 ± 0.43%, $p = 0.002$; respectively), as did the Autograft group (10.953 ± 0.98%, $p = 0.005$, $p = 0.001$, respectively) and the NCSC group (8.53 ± 0.08%, $p = 0.047$, $p = 0.011$, respectively). There was no significant difference between the NCSC + ES group and the Autograft group ($p > 0.05$).

3.3.4. Myelin thickness—At 6 weeks, the myelin thickness of the empty conduit group (0.69 ± 0.07 μm) is lower than all other groups ($p < 0.001$). In addition, the myelin thickness of the NCSC + ES group (1.60 ± 0.13 μm) is significantly greater than the ES only group (1.09 ± 0.16 μm, $p < 0.05$). There was no significant difference between the NCSC + ES and autograft groups. At 12 weeks, the empty conduit group (0.56 ± 0.06 μm) has the significantly lower myelin thickness than all other groups ($p < 0.001$), and no difference is observed between the NCSC + ES (2.11 ± 0.09 μm) and autograft groups (1.75 ± 0.15 μm).

3.4. Combined ES and NCSC therapy improved nerve conductivity

Overall across all time points, the autograft group had a larger number of rats with discernible signals than any other group (8 of 12 for CMAP, 6 of 12 for MEP). The difference for CMAP signals was significant when comparing the autograft group with CTL, ES, and NCSC groups ($p < 0.05$). There was a higher number ($p > 0.05$) of discernible signals in the NCSC + ES group (3 of 12 for CMAP, 2 of 12 for MEP) compared to the NCSC group (1/12 for CMAP and MEP), the ES group (1/12 for CMAP), and CTL group (no discernible signals). Amplitude and latency data were not evaluated due to the small number of rats showing discernible signals.

3.5. Muscle atrophy was attenuated with combined ES and NCSC therapy

After nerve transection, neuromuscular innervation was reduced and the denervated gastrocnemius muscles were atrophied. The CTL and ES groups have significantly smaller muscles after 12 weeks of recovery (Fig. 7A). Observation of fiber crosssectional area (Fig.

7B) revealed that gastrocnemius from CTL group has significantly smaller fibers with irregular shapes. In the ES and NCSC groups, muscles show a mix of fibers with varying sizes. In contrast, ES + NCSC and autograft muscles have homogenously distributed fiber diameters with a regular shape.

The gastrocnemius muscle weight measurement demonstrated that NCSC + ES treatment resulted in comparable outcomes to the autograft group on muscle mass preservation after denervation after both 6 and 12 weeks (Fig. 7C). At both time points, no statistical difference of GMI was observed between the NCSC + ES group and the autograft groups ($p > 0.05$). At 6 weeks, NCSC + ES group had the highest GMI (0.38 ± 0.03) when compared with autograft (0.32 ± 0.07; $p > 0.05$), NCSC (0.23 ± 0.03; $p < 0.01$), ES (0.15 ± 0.02; $p < 0.01$), and CTL(0.16 ± 0.04; $p < 0.01$) groups. At 12 weeks, NCSC + ES (0.29 ± 0.06) and autograft (0.29 ± 0.04) groups were comparable ($p > 0.05$), and both had significantly higher GMI than ES (0.15 ± 0.02; $p < 0.05$ for both) and CTL (0.016 ± 0.01; $p < 0.05$ for both) groups, but not the NCSC group (0.23 ± 0.05; $p > 0.05$). The ES group was not significantly different at either time point from the CTL group ($p > 0.05$).

3.6. Transplantation of NCSCs and application of ES promoted functional gait recovery

3.6.1. Representative footprints—In uninjured animals, the forepaw and hindpaw footprints perfectly coordinated with each other (Fig. 8A). 12 weeks after injury, the footprints of the forepaw and hindpaw were frequently mismatched. For the control (CTL) and ES groups, the prints of injured feet decreased to half of the uninjured feet, and print areas were decreased as well. For the NCSC only group, the injured footprints showed improvements over control, but print areas were still smaller than control. The NCSC + ES and autograft groups had similar outcomes, with the fore and hind paws starting to coordinate with increasing print areas.

3.6.2. Stand time (Fig. 8B)

Overall across all time points, the NCSC + ES group showed significant improvement (with longer stand time) over the NCSC, ES, and CTL groups ($p = 0.002$, $p = 0.001$, $p < 0.001$, respectively). The Autograft group was also significantly better than the NCSC, ES and CTL groups ($p = 0.046$, $p = 0.015$, $p = 0.009$, respectively), with no significant difference with the NCSC + ES group ($p > 0.05$).

At 6 weeks, the NCSC + ES group ($72.05 \pm 1.45\%$) showed significant improvement over the NCSC, ES, and CTL groups ($60.53 \pm 1.30\%$, $p = 0.009$; $54.91 \pm 2.79\%$, $p < 0.001$; $54.98 \pm 4.18\%$, $p < 0.001$; respectively). The Autograft group ($72.04 \pm 4.64\%$) also showed significantly better results than the NCSC, ES, and CTL groups ($p = 0.010$, $p = 0.001$, $p < 0.001$, respectively). There was no significant difference between the NCSC + ES group and the autograft group ($p > 0.05$). At 12 weeks, the NCSC + ES group ($76.71 \pm 2.33\%$) also showed significant improvement over the NCSC, ES, and CTL groups ($63.49 \pm 3.54\%$, $p = 0.018$; $57.38 \pm 5.99\%$, $p = 0.002$; $58.67 \pm 3.87\%$, $p = 0.002$; respectively), and the Autograft group ($72.63 \pm 2.84\%$) showed significant improvement over the ES and CTL groups ($p = 0.013$, $p = 0.018$, respectively). There was no significant difference between the NCSC + ES group and the autograft group ($p > 0.05$).

3.6.3. Duty cycle (Fig. 8C)—Overall, the duty cycle metric revealed that the animals in the NCSC + ES group showed significantly higher results than the NCSC and CTL groups ($p = 0.016$, $p = 0.005$, respectively) indicating better functional recovery. The autograft group only showed significantly higher results than the CTL group ($p = 0.035$). The NCSC + ES group showed no significant difference with the Autograft group ($p > 0.05$).

At 6 weeks, the NCSC + ES group (72.17 ± 1.68%) showed significant improvement over the CTL group (61.01 ± 3.55%, $p = 0.008$), while the Autograft group (74.10 ± 3.05%) showed significant improvement over the ES and CTL groups (64.88 ± 4.05%, $p = 0.039$; $p = 0.003$; respectively). No significant differences were found between the NCSC + ES group and the NCSC group (67.25 ± 2.36%, $p > 0.05$) or Autograft group ($p > 0.05$). At 12 weeks, the NCSC + ES group (76.96 ± 2.99%) showed significant improvement over the NCSC, ES, and CTL groups (63.91 ± 4.09%, $p = 0.026$; 64.35 ± 5.74%, $p = 0.038$; 64.24 ± 4.27%, $p = 0.029$; respectively). No significant difference existed between the autograft group (73.67 ± 2.08%) and any other group ($p > 0.05$).

4. Discussion

We developed and optimized a novel cell-based therapeutic approach by augmenting stem cell transplantation with optimal ES for the repair of critical-sized nerve gaps. Compared to previous *in vitro* stimulators, our made-in-house ES device features an *in vitro* 96-well culture plate that permits easy modulation of multiple parameters and an *in vivo* vertical configuration stimulator able to stimulate a larger area (and separate the effects of galvanic migration). Using our made-in-house setup, we showed that NCSCs must be cultured on cathodes for NCSC differentiation, and that ES can promote SC differentiation *in vitro.* We further identified that optimal ES significantly promoted the proliferation and differentiation of NCSC into SCs both *in vitro* and *in vivo,* and boosted the therapeutic effect of nerve regeneration. The nerve regeneration efficiency of NCSC transplantation combined with ES was comparable to that of autograft implantation and superior to that of NCSC transplantation alone.

NCSCs have been investigated *in vitro* and *in vivo* in several studies for peripheral nerve repair [41,42], but outcomes have been largely unsatisfactory and treatment with NCSCs alone is still limited when compared to autologous nerve grafts. While NCSC and ES treatments have been individually tested for peripheral nerve regeneration in the past, clinical outcomes have been suboptimal. Our experiment indicated that transplantation of NCSCs alone can elicit incremental but limited improvements in functional recovery, and ES alone did not show significant differences compared to the CTL group in our critical-sized nerve repair model. The NCSC group was only able to show significant improvements compared to the CTL group, and had inferior outcomes when compared to the autograft group. ES on NCSC transplantation facilitates both synergistic and complementary effects that amount to outcomes comparable to those of the autograft group after conducting immunofluorescence analysis, histomorphometric assessment, electrophysiological testing, behavioral gait tests, and gastrocnemius muscle index measurements.

NCSCs are thought to exert therapeutic effects by giving rise to SC precursors [8], however, there is strong evidence showing that the survival of SC precursors is dependent on axonal survival signals [43], and SCs die rapidly *in vitro* even when plated at a very high density [44]. ES alters the local electrical field [45], enhances the release of nerve growth factors from SCs [46], promotes the induction of neurotrophins release [15], and enhances the proliferation and functional activity of SCs *in vitro.* ES was shown to enhance the release of nerve growth factor and brain-derived neurotrophic factor from Schwann cells in a calcium-dependent mechanism [46]. However, the effect of ES on transplanted NCSCs remain unknown. Our results show that ES may have positively impacted stem cell survival and differentiation, and provide a beneficial synergistic effect.

Our immunohistochemistry testing showed higher a higher number of viable NCSCs and SC differentiation in the NCSC + ES group when compared to the NCSC group, indicating that ES significantly increases the proliferation and differentiation transplanted NCSCs *in vivo.* This also confirms that improved regenerative outcomes are associated with an increased abundance of both NCSCs and SCs, and that optimized ES contributes to increased cell number and differentiation of transplanted stem cells *in vivo.* As NCSCs are known to either secrete growth factors or modulate endogenous secretion of growth factors from SCs [8,47], transplanted NCSCs may also serve as reservoirs of neurotrophic factors which support SCs function. Axon—SC interactions mediated by neurotrophic factors likely play a pivotal role in peripheral nerve regeneration. This beneficial effect may also be a result of increased NCSCs (either direct from ES or indirect from ES enhancing axonal regrowth/neurotrophic production). One limitation of this study is the lack of DNA/RNA analysis, which is one of the preferred methods for characterizing stem cell differentiation. Thus the detailed mechanism of the action of NCSCs on nerve regeneration and further characterization of stem cell differentiation awaits future investigation.

Our results clearly showed that ES on NCSC transplantation enhanced locomotion, increased muscle weights, increased myelinated axons. However, while the electrophysiological data showed a positive trend, the improvement was not statistically different. Our group has extensive experience with electrophysiological studies in nerve injury, including short-term and long-term (up to 9 months) neuro-behavioral outcomes, ES, stem cell therapy, and evoked potential preclinical (in rabbit and rat) and clinical studies [28–31,48–50]. Unlike nerve crush injury or other mild/ moderate nerve injury where electrophysiology assessment is an effective method to evaluate functional recovery of the regenerated nerve, our experience is that the regeneration process is highly variably expressed on electrophysiological testing in critical-sized nerve repair models which may due to the asymmetric regeneration process in the nerve scaffold. This may further underlie the potential limitation for electrophysiological studies, and larger sample sizes (therefore more animals) may be needed to obtain sufficient statistical power to detect the true difference in recovery [51].

While conductive conduits have shown the ability to induce neuronal differentiation of PC12 cells in vivo [52] and promoting sciatic nerve regeneration in rat models by transmitting self-originated electrical stimulation between cells [53], in our study, we used external electrical stimulation on transplanted NCSCs to promote the Schwann cell differentiation and nerve

regeneration. The polycaprolactone nanofiber we used is not a conductive material; however, the hydrogel + PBS filling is. Furthermore, a nonconductive nerve scaffold will isolate the electrical signals from surrounding tissues, such as muscle or other nerve tissue. Comparing previous studies using percutaneous electrical stimulation which stimulates a large surrounding area and superficial overlying muscles without accurate location of deep targets [54,55], our method provides a more precise effect on the transplanted stem cell.

While we used xenotransplantation of human ESC derived NCSCs in our animal experiments (which may be suboptimal to autologous transplantation), using human stem cells in pre-clinical studies further ensures the potential for clinical translation [56] as human and animal stem cells might have different biological characteristics. Our results can still be reliably interpreted for validation of electrostimulation's effect on human NCSCs, which may be generalizable to NCSCs of from other sources. Compared to other stem cells derived from adult organisms, our fibroblast- derived NCSCs are much younger, less invasive, better isolated, and impart high clinical translational value [22,57]. Our team has established a direct methodology for converting patient fibroblasts into "induced neural crest (iNC)" [58], which may have better translational value pending further studies. Overall, our protocols mimic the clinical environment, and can be readily combined with stem cell therapy at the time of nerve repair. Thus, our novel treatment has a high translational potential for patients with peripheral nerve trauma requiring surgical repairs, making it a very attractive option for peripheral nerve surgeons in the future. The present study provides primary evidence that treatment of peripheral nerve injuries with NCSC transplantation and ES holds great potential and is well positioned to have wide clinical applicability. Future preclinical studies in large animals or phase I clinical trials are needed to further optimize this cell-based intervention for clinical use, and may elucidate the mechanisms underlying the synergism of NSCS and ES.

5. Conclusion

In summary, with our custom-made 96 well ES platform, we showed that ES can promote NCSC differentiation in *vitro* when cultured on cathodes, and identified optimal ES parameters for SC differentiation. With our findings from the in *vitro* ES optimization experiments, we developed a novel cell-based therapy for critical-sized nerve repair, and demonstrated beneficial effects of optimized ES on NCSC transplantation in a sciatic nerve injury model. We found that ES on NCSC transplantation has synergistic and complementary effects that are able to promote regeneration across large nerve gaps with results comparable to autografts. This synergy may be due to improved survival and differentiation of transplanted NCSCs *in vivo* following ES. This novel cell-based intervention presents an effective and safe approach for better outcomes after peripheral nerve repair.

Supplementary Material

Refer to Web version on PubMed Central for supplementary material.

Acknowledgment

This study was supported by Maryland Stem Cell Research Fund, USA (2013-MSCRFE-146–00, 2018-MSCRFD-4271) (both to XJ), RO1HL118084 and R01NS110387 from United States National Institutes of Health (NIH) (both to XJ). Mao was supported by National Science Foundation, USA (DMR1410240, to Mao).

References

[1]. Grinsell D, Keating CP, Peripheral nerve reconstruction after injury: a review of clinical and experimental therapies, BioMed Res. Int 2014 (2014), 698256. [PubMed: 25276813]

[2]. Jia X, Romero-Ortega MI, Teng YD, Peripheral nerve regeneration: mechanism, cell biology, and therapies, BioMed Res. Int 2014 (2014), 145304. [PubMed: 25587530]

[3]. Jones S, Eisenberg HM, Jia X, Advances and future applications of augmented peripheral nerve regeneration, Int. J. Mol. Sci 17 (9) (2016) 1494.

[4]. Lewitus D, Vogelstein RJ, Zhen G, Choi YS, Kohn J, Harshbarger S, Jia X, Designing tyrosine-derived polycarbonate polymers for biodegradable regenerative type neural interface capable of neural recording, IEEE Trans. Neural Syst. Rehabil. Eng 19 (2) (2011) 204–212. [PubMed: 21147598]

[5]. Eftekhar T, Teimoory N, Miri E, Nikfallah A, Naeimi M, Ghajarzadeh M, Posterior tibial nerve stimulation for treating neurologic bladder in women: a randomized clinical trial, Acta Med. Iran 52 (11) (2014) 816–821. [PubMed: 25415813]

[6]. Johnson BN, Lancaster KZ, Zhen GH, He JY, Gupta MK, Kong YL, Engel EA, Krick KD, Ju A, Meng FB, Enquist LW, Jia XF, McAlpine MC, 3D printed anatomical nerve regeneration pathways, Adv. Funct. Mater 25 (39) (2015) 6205–6217. [PubMed: 26924958]

[7]. Bryson JB, Machado CB, Crossley M, Stevenson D, Bros-Facer V, Burrone J, Greensmith L, Lieberam I, Optical control of muscle function by transplantation of stem cell-derived motor neurons in mice, Science 344 (6179) (2014) 94–97. [PubMed: 24700859]

[8]. Wang A, Tang Z, Park IH, Zhu Y, Patel S, Daley GQ, Li S, Induced pluripotent stem cells for neural tissue engineering, Biomaterials 32 (22) (2011) 5023–5032. [PubMed: 21514663]

[9]. Jiang L, Jones S, Jia X, Stem cell transplantation for peripheral nerve regeneration: current options and opportunities, Int. J. Mol. Sci 18 (1) (2017) 94.

[10]. Walsh S, Midha R, Practical considerations concerning the use of stem cells for peripheral nerve repair, Neurosurg. Focus 26 (2) (2009) E2.

[11]. McCaig CD, Rajnicek AM, Song B, Zhao M, Controlling cell behavior electrically: current views and future potential, Physiol. Rev 85 (3) (2005) 943–978. [PubMed: 15987799]

[12]. Chang KA, Kim JW, Kim JA, Lee SE, Kim S, Suh WH, Kim HS, Kwon S, Kim SJ, Suh YH, Biphasic electrical currents stimulation promotes both proliferation and differentiation of fetal neural stem cells, PLoS One 6 (4) (2011), e18738. [PubMed: 21533199]

[13]. Park SY, Park J, Sim SH, Sung MG, Kim KS, Hong BH, Hong S, Enhanced differentiation of human neural stem cells into neurons on graphene, Adv. Mater 23 (36) (2011) H263–H267. [PubMed: 21823178]

[14]. Yamada M, Tanemura K, Okada S, Iwanami A, Nakamura M, Mizuno H, Ozawa M, Ohyama-Goto R, Kitamura N, Kawano M, Tan-Takeuchi K, Ohtsuka C, Miyawaki A, Takashima A, Ogawa M, Toyama Y, Okano H, Kondo T, Electrical stimulation modulates fate determination of differentiating embryonic stem cells, Stem Cell. 25 (3) (2007) 562–570.

[15]. Kim IS, Song YM, Cho TH, Pan H, Lee TH, Kim SJ, Hwang SJ, Biphasic electrical targeting plays a significant role in schwann cell activation, Tissue Eng. 17 (9–10) (2011) 1327–1340.

[16]. Shen J, Duan XH, Cheng LN, Zhong XM, Guo RM, Zhang F, Zhou CP, Liang BL, In vivo MR imaging tracking of transplanted mesenchymal stem cells in a rabbit model of acute peripheral nerve traction injury, J. Magn. Reson. Imag 32 (5) (2010) 1076–1085.

[17]. Huang J, Hu X, Lu L, Ye Z, Wang Y, Luo Z, Electrical stimulation accelerates motor functional recovery in autograft-repaired 10 mm femoral nerve gap in rats, J. Neurotrauma 26 (10) (2009) 1805–1813. [PubMed: 19226192]

[18]. Gordon T, Amirjani N, Edwards DC, Chan KM, Brief post-surgical electrical stimulation accelerates axon regeneration and muscle reinnervation without affecting the functional measures in carpal tunnel syndrome patients, Exp. Neurol 223 (1) (2010) 192–202. [PubMed: 19800329]

[19]. Wake H, Lee PR, Fields RD, Control of local protein synthesis and initial events in myelination by action potentials, Science 333 (6049) (2011) 1647–1651. [PubMed: 21817014]

[20]. Pavesi A, Adriani G, Rasponi M, Zervantonakis IK, Fiore GB, Kamm RD, Controlled electromechanical cell stimulation on-a-chip, Sci. Rep 5 (2015) 11800. [PubMed: 26135970]

[21]. McCaig CD, Rajnicek AM, Song B, Zhao M, Controlling cell behavior electrically: current views and future potential, Physiol. Rev 85 (3) (2005) 943–978. [PubMed: 15987799]

[22]. Lee G, Kim H, Elkabetz Y, Al Shamy G, Panagiotakos G, Barberi T, Tabar V, Studer L, Isolation and directed differentiation of neural crest stem cells derived from human embryonic stem cells, Nat. Biotechnol 25 (12) (2007) 1468–1475. [PubMed: 18037878]

[23]. Zhang, Zachary SW, Ren Yongjuan, Lee Gabsang, Zeng Xianmin, Hoke Ahmet, Ming Guoli, Mao Hai-Quan, Electric stimulation promotes the neuronal differentiation of human ESC-derived neural crest stem cells and neural stem cells, in: The 4th Annual Maryland Stem Cell Research Symposium, Towson, Maryland, 2011, p. 43.

[24]. Lu MC, Ho CY, Hsu SF, Lee HC, Lin JH, Yao CH, Chen YS, Effects of electrical stimulation at different frequencies on regeneration of transected peripheral nerve, Neurorehabilitation Neural Repair 22 (4) (2008) 367–373. [PubMed: 18663248]

[25]. Loeb GE, Marks WB, Hoffer JA, Cat hindlimb motoneurons during locomotion. IV. Participation in cutaneous reflexes, J. Neurophysiol 57 (1987) 563–573. [PubMed: 3559693]

[26]. Pires F, Ferreira Q, Rodrigues CA, Morgado J, Ferreira FC, Neural stem cell differentiation by electrical stimulation using a cross-linked PEDOT substrate: expanding the use of biocompatible conjugated conductive polymers for neural tissue engineering, Biochim. Biophys. Acta 1850 (6) (2015) 1158–1168. [PubMed: 25662071]

[27]. Chew SY, Mi R, Hoke A, Leong KW, Aligned protein-polymer composite fibers enhance nerve regeneration: a potential tissue-engineering platform, Adv. Funct. Mater 17 (8) (2007) 1288–1296. [PubMed: 18618021]

[28]. Jia X, Chen Z, Zhang J, Chen T, Zhu Y, Han R, The application of modified intrafascicular electrodes in recording the electric signal of sciatic nerve of rabbits, Shanghai Medical Journal 26 (4) (2003) 243–245.

[29]. Jia X, Koenig MA, Zhang X, Zhang J, Chen T, Chen Z, Residual motor signal in long-term human severed peripheral nerves and feasibility of neural signal-controlled artificial limb, J Hand Surg [Am] 32 (5) (2007) 657–666.

[30]. Jia X, Zhang J, Chen T, Chen Z, Zhu Y, Han R, Qiu Z, Experimental study on harvesting the electric signal of peripheral nerve at rabbits by intrafascicular microelectrodes, Chinese Journal of Hand Surgery 18 (4) (2002) 245–247.

[31]. Jia X, Zhen G, Puttgen A, Zhang J, Chen T, Improved long-term recording of nerve signal by modified intrafascicular electrodes in rabbits, Microsurgery 28 (3) (2008) 173–178. [PubMed: 18286654]

[32]. McCloy RA, Rogers S, Caldon CE, Lorca T, Castro A, Burgess A, Partial inhibition of Cdk1 in G2 phase overrides the SAC and decouples mitotic events, Cell Cycle 13 (9) (2014) 1400–1412. [PubMed: 24626186]

[33]. Du J, Chen H, Zhou K, Jia X, Quantitative multimodal evaluation of passaging human neural crest stem cells for peripheral nerve regeneration, Stem Cell Rev. 14 (1) (2018) 92–100. [PubMed: 28780695]

[34]. Ikeda M, Oka Y, The relationship between nerve conduction velocity and fiber morphology during peripheral nerve regeneration, Brain Behav 2 (4) (2012) 382–390. [PubMed: 22950042]

[35]. Wu D, Xiong W, Jia XF, Geocadin RG, Thakor NV, Short- and long-latency somatosensory neuronal responses reveal selective brain injury and effect of hypothermia in global hypoxic ischemia, J.Neurophysiol 107 (4) (2012) 1164–1171. [PubMed: 22157111]

[36]. Jiang W, Wang Y, Tang J, Peng J, Wang Y, Guo Q, Guo Z, Li P, Xiao B, Zhang J, Low-intensity pulsed ultrasound treatment improved the rate of autograft peripheral nerve regeneration in rat, Sci. Rep 6 (2016) 22773. [PubMed: 27102358]

[37]. Zhen G, Wen C, Jia X, Li Y, Crane JL, Mears SC, Askin FB, Frassica FJ, Chang W, Yao J, Carrino JA, Cosgarea A, Artemov D, Chen Q, Zhao Z, Zhou X, Riley L, Sponseller P, Wan M, Lu WW, Cao X, Inhibition ofTGF-beta signaling in mesenchymal stem cells of subchondral bone attenuates osteoarthritis, Nat. Med 19 (6) (2013) 704–712. [PubMed: 23685840]

[38]. Chen H, Du J, Zhang Y, Barnes K, Jia X, Establishing a reliable gait evaluation method for rodent studies, J. Neurosci. Meth 283 (2017) 92–100.

[39]. Al-Majed AA, Neumann CM, Brushart TM, Gordon T, Brief electrical stimulation promotes the speed and accuracy of motor axonal regeneration, J. Neurosci 20 (7) (2000) 2602–2608. [PubMed: 10729340]

[40]. Gordon T, Brushart TM, Chan KM, Augmenting nerve regeneration with electrical stimulation, Neurol. Res 30 (10) (2008) 1012–1022. [PubMed: 19079975]

[41]. Lee EJ, Xu L, Kim GH, Kang SK, Lee SW, Park SH, Kim S, Choi TH, Kim HS, Regeneration of peripheral nerves by transplanted sphere of human mesenchymal stem cells derived from embryonic stem cells, Biomaterials 33 (29) (2012) 7039–7046. [PubMed: 22795857]

[42]. Jiang L, Jones S, Jia X, Stem cell transplantation for peripheral nerve regeneration: current options and opportunities, Int. J. Mol. Sci 18 (1) (2017).

[43]. Mirsky R, Jessen KR, Brennan A, Parkinson D, Dong Z, Meier C, Parmantier E, Lawson D, Schwann cells as regulators of nerve development, J. Physiol. Paris 96 (1–2) (2002) 17–24. [PubMed: 11755779]

[44]. Jessen KR, Brennan A, Morgan L, Mirsky R, Kent A, Hashimoto Y, Gavrilovic J, The Schwann cell precursor and its fate: a study of cell death and differentiation during gliogenesis in rat embryonic nerves, Neuron 12 (3) (1994) 509–527. [PubMed: 8155318]

[45]. Vats K, Benoit DS, Dynamic manipulation of hydrogels to control cell behavior: a review, Tissue Eng. B Rev 19 (6) (2013) 455–469.

[46]. Yan X, Liu J, Ye Z, Huang J, He F, Xiao W, Hu X, Luo Z, CaMKII-mediated CREB phosphorylation is involved in Ca2+-Induced BDNF mRNA transcription and neurite outgrowth promoted by electrical stimulation, PLoS One 11 (9) (2016), e0162784. [PubMed: 27611779]

[47]. Sakaue M, Sieber-Blum M, Human epidermal neural crest stem cells as a source of Schwann cells, Development 142 (18) (2015) 3188–3197. [PubMed: 26251357]

[48]. Jia X, Chen T, Chen Z, Zhang J, Zhang X, Si Y, Hu T, Gao Z, Yang Y, The original report of the first experimental study on electric prosthesis controlled by signals of nerves in amputation stump of human, Chinese Journal of Physical Medicine and Rehabilitation 26 (1) (2004) 20–23.

[49]. Jia X, Chen Z, Chen T, Zhang J, Zhang X, Si Y, Hu T, Harvesting the signals of nerves in the remaining limb of human by intrafascicular microelectrodes, Chinese Journal of Microsurgery 27 (1) (2004) 24–26.

[50]. Zhen G, Chen H, Tsai SY, Zhang J, Chen T, Jia X, Long-term feasibility and biocompatibility of directly microsurgically implanted intrafascicular electrodes in free roaming rabbits, J. Biomed. Mater. Res. B Appl. Biomater (2018 4 19), 10.1002/jbm.b.34135 [Epub ahead of print], www.ncbi.nlm.nih.gov/pubmed/29675920.

[51]. Li R, Li Y, Wu Y, Zhao Y, Chen H, Yuan Y, Xu K, Zhang H, Lu Y, Wang J, Li X, Jia X, Xiao J, Heparin-poloxamer thermosensitive hydrogel loaded with bFGF and NGF enhances peripheral nerve regeneration in diabetic rats, Biomaterials 168 (2018) 24–37. [PubMed: 29609091]

[52]. Shi Z, Gao H, Feng J, Ding B, Cao X, Kuga S, Wang Y, Zhang L, Cai J, In situ synthesis of robust conductive cellulose/polypyrrole composite aerogels and their potential application in nerve regeneration, Angew Chem. Int. Ed. Engl 53 (21) (2014) 5380–5384. [PubMed: 24711342]

[53]. Zhou Z, Zhang F, Wang J-G, Chen Q-C, Yang W-Z, He N, Jiang Y, Chen F, Liu JJ, Electrospinning of PELA/PPY fibrous conduits: promoting peripheral nerve regeneration in rats by self-originated electrical stimulation, ACS Biomater. Sci. Eng 2 (9) (2016) 1572–1581.

[54]. Chen YS, Hu CL, Hsieh CL, Lin JG, Tsai CC, Chen TH, Yao CH, Effects of percutaneous electrical stimulation on peripheral nerve regeneration using silicone rubber chambers, J. Biomed. Mater. Res 15 (57) (2001) 541–549.

[55]. Lu MC, Tsai CC, Chen SC, Tsai FJ, Yao CH, Chen YS, Use of electrical stimulation at different current levels to promote recovery after peripheral nerve injury in rats, J. Trauma 67 (5) (2009) 1066–1072. [PubMed: 19901670]

[56]. Harding J, Mirochnitchenko O, Preclinical studies for induced pluripotent stem cell-based therapeutics, J. Biol. Chem 289 (8) (2014) 4585–4593. [PubMed: 24362021]

[57]. Lee G, Chambers SM, Tomishima MJ, Studer L, Derivation of neural crest cells from human pluripotent stem cells, Nat. Protoc 5 (4) (2010) 688–701. [PubMed: 20360764]

[58]. Kim YJ, Lim H, Li Z, Oh Y, Kovlyagina I, Choi IY, Dong X, Lee G, Generation of multipotent induced neural crest by direct reprogramming of human postnatal fibroblasts with a single transcription factor, Cell Stem Cell 15 (4) (2014) 497–506. [PubMed: 25158936]

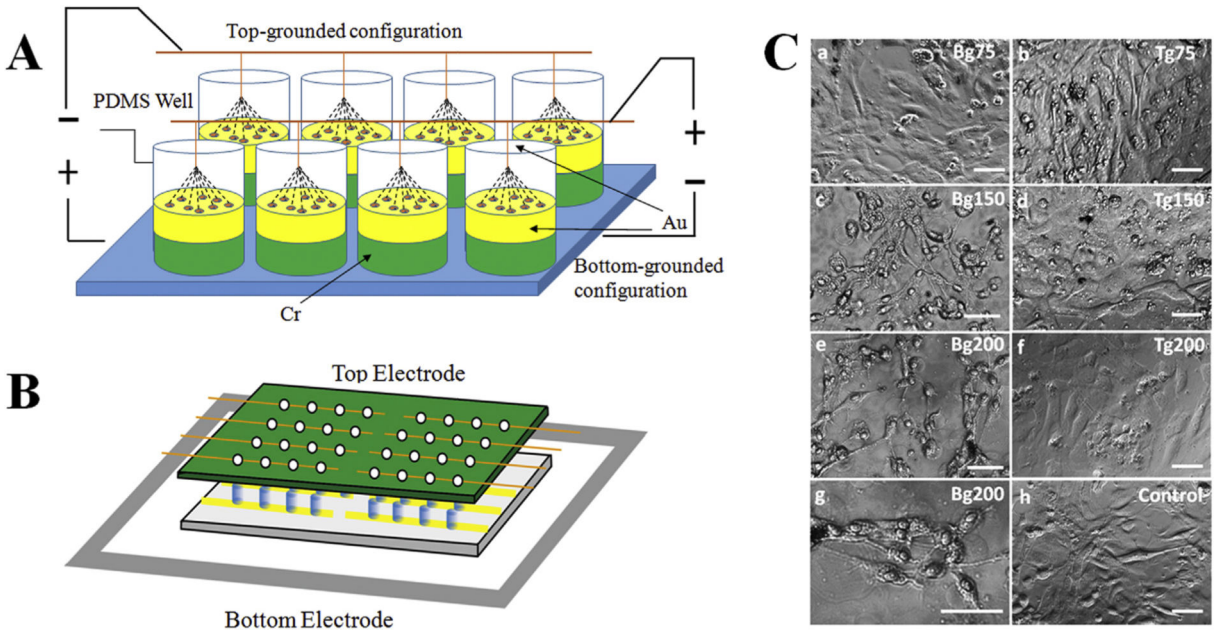

Fig. 1.

(A) Illustration of the electrostimulation platform, which permits easy and simultaneous modulation of multiple parameters such as field polarity, electrical potential, pulsing frequency, and stimulation duration, to deliver adjustable electrical outputs to cells in individual wells. (B) Side view of stimulation set up. Each condition has one group of 4 electrically connected wells. Top electrodes are replaced with clean sealing film when no stimulation is applied. (C) Phase images of NCSCs after stimulated with 1-Hz 50-ms pulses for 24 h at different potential gradients. Cells were stimulated with bottom-grounded (Bg) configuration (a, c, e, g) or top-grounded (Tg) configuration (b, d, f) at 75, 150 and 200 mV/mm potential in comparison with cells without electrostimulation (h). (g) shows a higher magnification image of (e). Scale bars represent 100 μm.

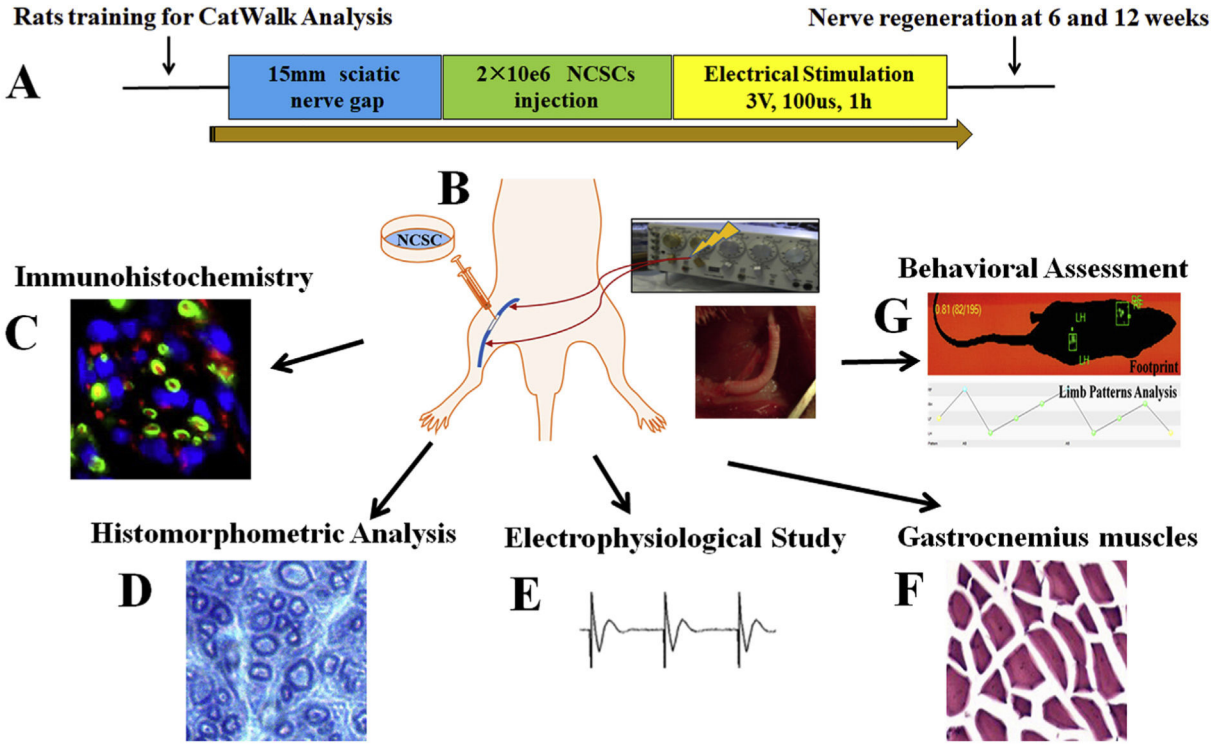

Fig. 2.

(A) Animal experimental design and procedures; (B) hNCSCs were injected into nerve conduit and ES was applied after 15 mm sciatic nerve repair to promote nerve regeneration. (C-G) Quantitative multimodal evaluation of nerve regeneration after hNCSC transplantation with electrical stimulation including immunohistochemistry (C), histomorphometric analysis (D), electrophysiological study (E), gastrocnemius muscle recovery (F), and behavioral assessment (G).

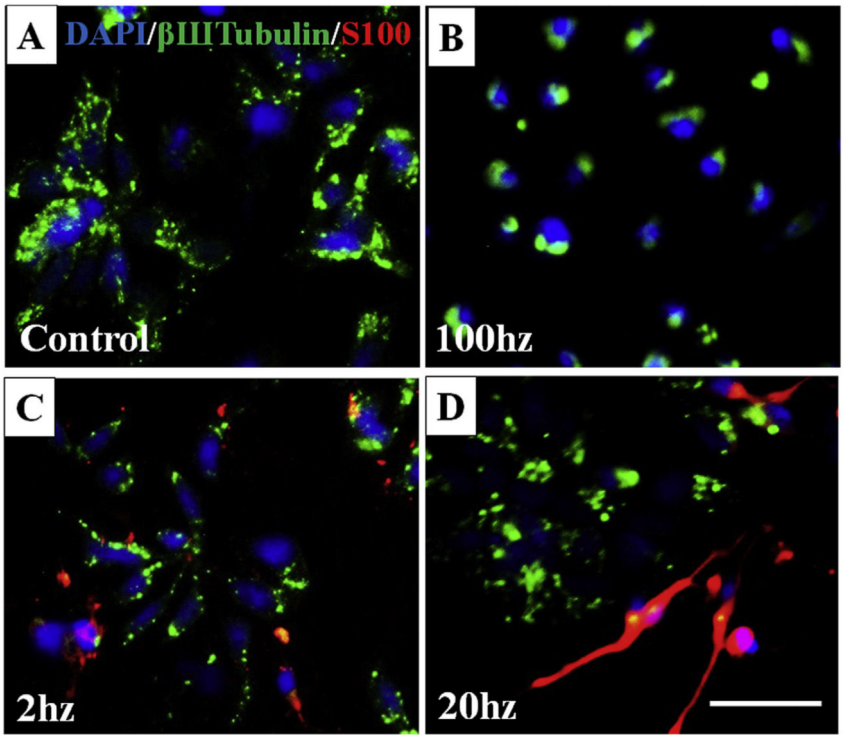

Fig. 3.

Immunofluorescent staining of bIII Tubulin (green) and S100 (red) showed an optimized electrical stimulation condition of 200 mV/mm, 100 ms, and 20hz, which best promoted Schwann's Cell (SC) differentiation by producing spindle-like SCs (D), compared to the other conditions of control without ES (A), 100 Hz (B), and 2 Hz (C). Scale bar = 20 μm. (For interpretation of the references to colour in this figure legend, the reader is referred to the Web version of this article.)

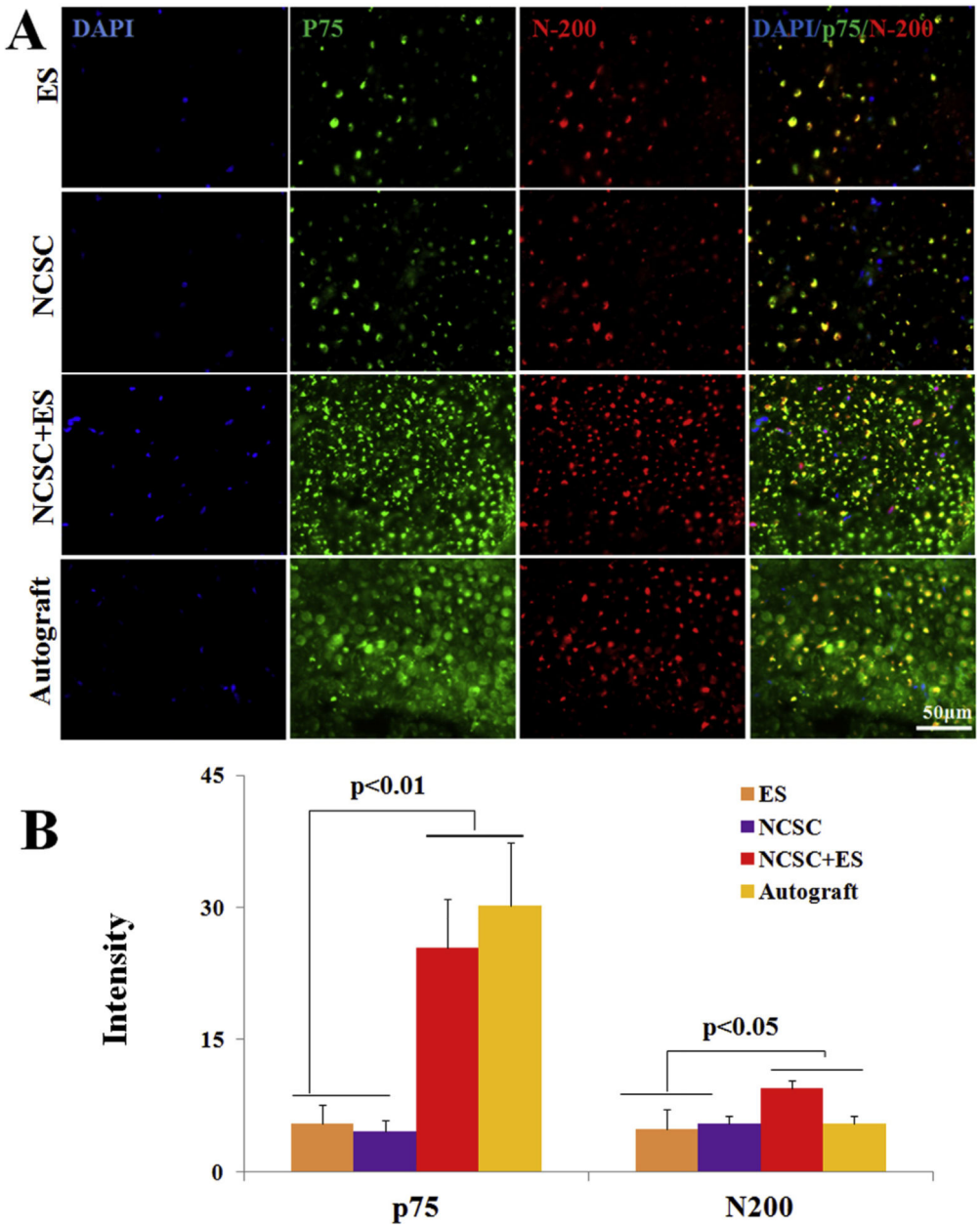

Fig. 4.

Representative cross-sectional immunofluorescence images after 12 weeks recovery, (A) the middle section of the nerve conduit was stained with DAPI (blue), p75 (green), and N-200 (red), scale bar = 50 μm; (B) comparison of the fluorescent intensity of p75 and N200, data are expressed as means ± SEM. N = 6 for each group. (For interpretation of the references to colour in this figure legend, the reader is referred to the Web version of this article.)

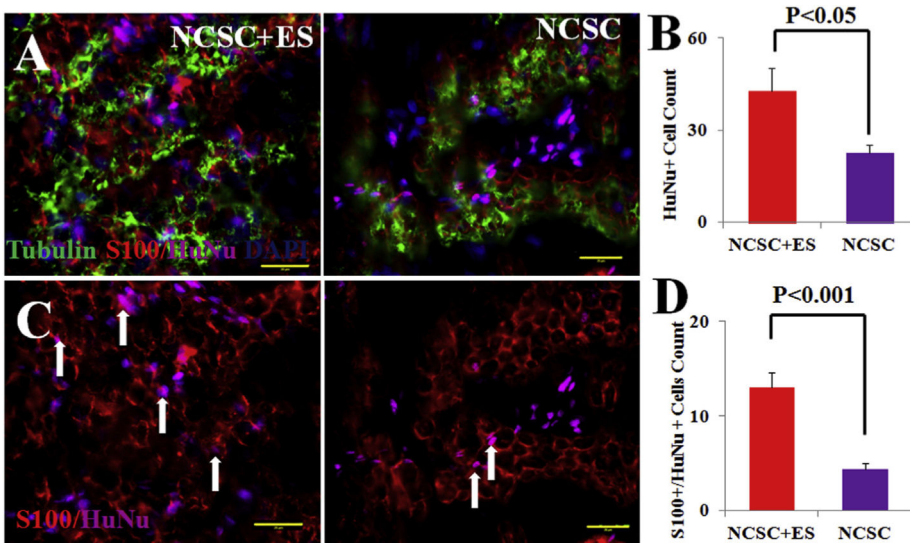

Fig. 5.

At 12 weeks, (A) hNCSC localization and differentiation were confirmed as evident by immunostaining of HuNu (magenta), S-100 (red), and Tubulin (green) in NCSC + ES and NCSC transplanted nerves; (B) qualification of HuNu positive cells showed that NCSC + ES has superior survivability than NCSC alone. (C) co-staining human cell nuclei (HuNu, magenta) and S-100 (red) expression indicated donor human cell-derived S100 positive cells (arrows) 12 weeks after NCSC transplantation; (D) qualification ofboth S100 and HuNu positive cells explained that hNCSCs were able to survive or differentiate into peripheral nerve support cells, and ES further promoted hNCSCs survival and differentiation in vivo. Blue = nuclear staining with DAPI. Scale bar represents 20 μm. (For interpretation of the references to colour in this figure legend, the reader is referred to the Web version of this article.)

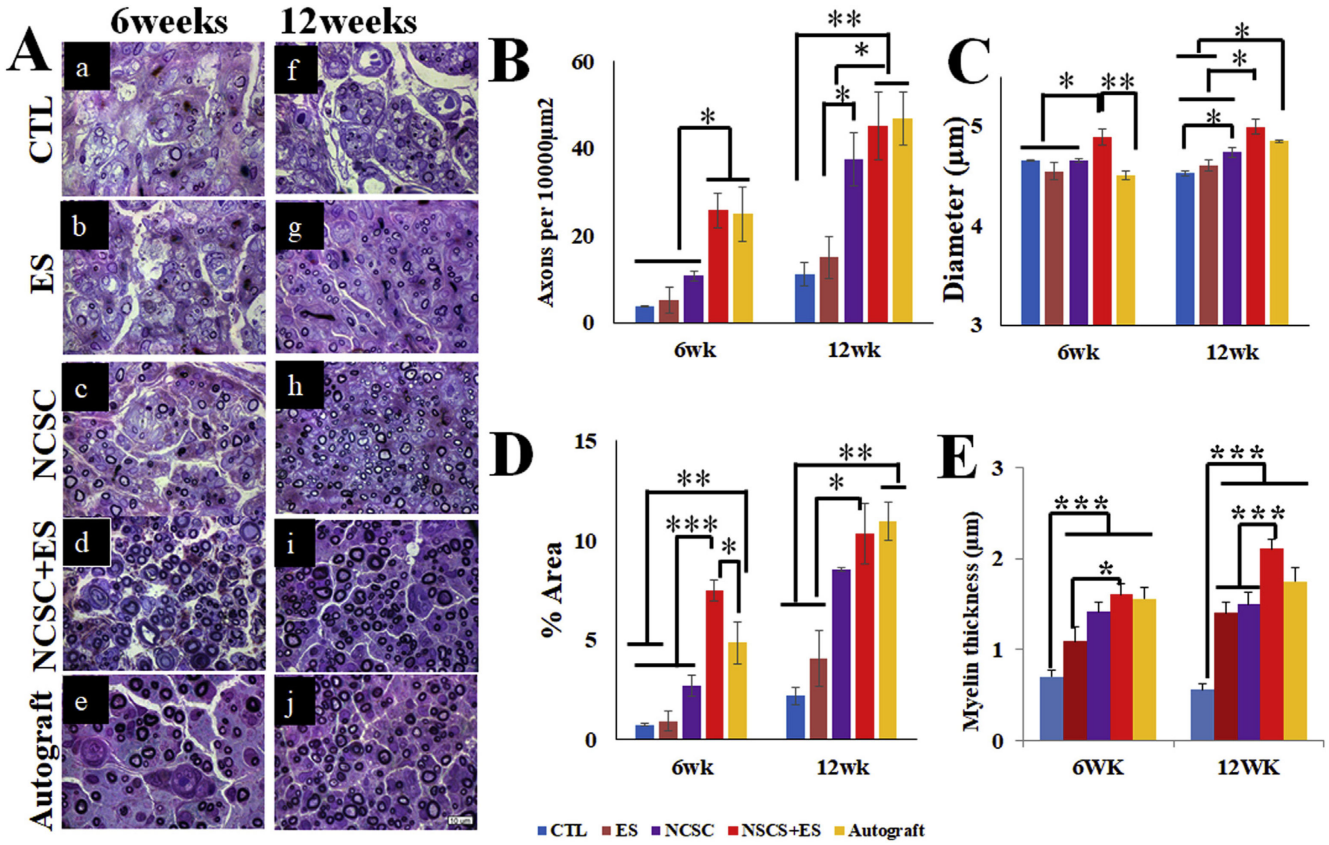

Fig. 6.

(A) Representative toluidine blue cross-section staining of sciatic nerves 6 weeks and 12 weeks after nerve repair from Control (CTL) (a, f), electrical stimulation (ES) (b, g), Neural crest stem cell (NCSC) (c, h), NCSC + ES (d, i), and autograft (e, j) groups. Images were taken under 1000 × magnification. NCSC + ES was superior to NCSC at both 6 and 12 weeks for the density of myelinated axons per 10,000 μm^2 in (B), the diameter of myelinated axons in (C), at 12 weeks for percentage of total area occupied by myelinated axons in (D), myelin thickness (fiber diameter (FD) - axon diameter (AD)). NCSC + ES was also superior to autografts for diameter at 6 weeks. Values represent means ± SEM. Scale bar = 10 μm ***$p < 0.001$, **$p < 0.01$, *$p < 0.05$.

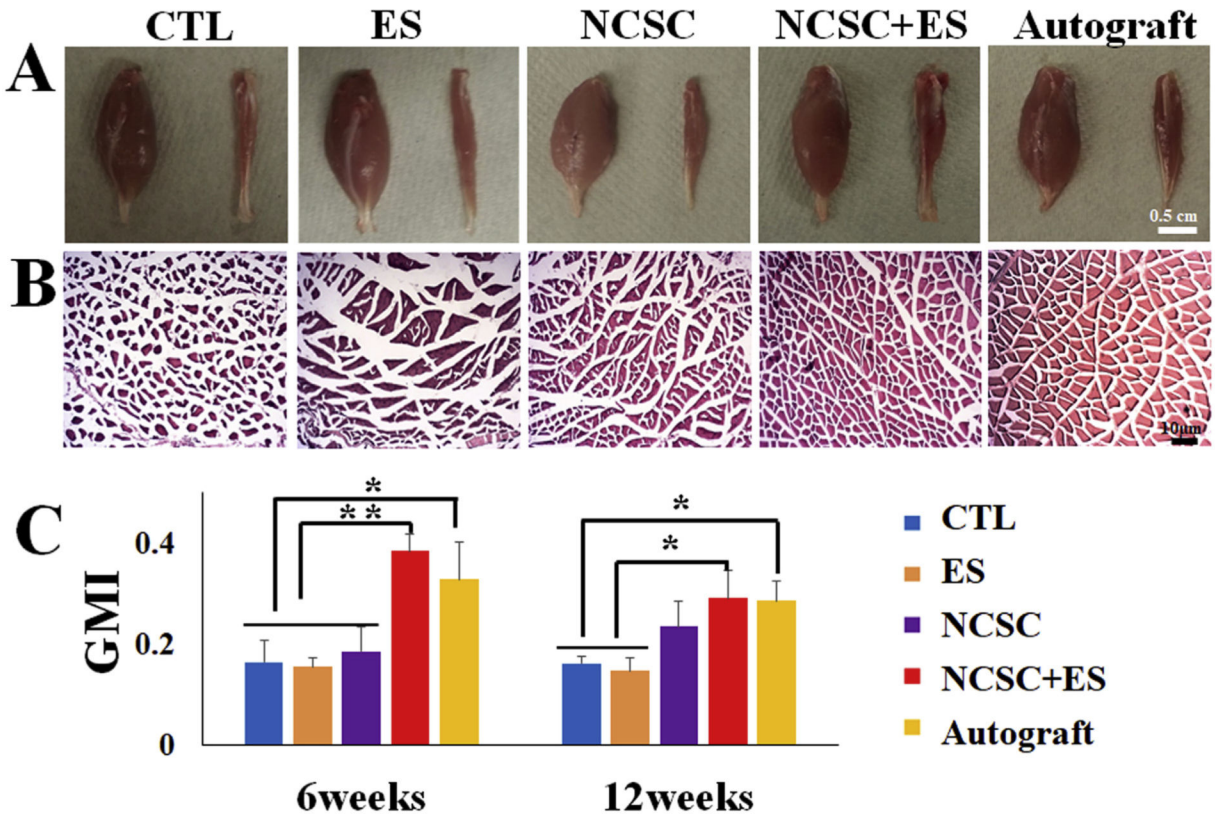

Fig. 7.

(A) Macroscopic view of the gastrocnemius muscles (scale bar = 0.5 cm) and (B) H&E staining of the gastrocnemius muscle in five groups at 12 weeks (scale bar = 10 μm). (C) *Gastrocnemius Muscle Index (GMI)* at 6 and 12 weeks after the surgery among groups. GMI was higher for Neural crest stem cell (NCSC) + electrical stimulation (ES) than autograft at both 6 and 12 weeks, without statistical difference. At 6 weeks, NCSC + ES had significantly higher GMI compared with NCSC, ES, and control (all $p < 0.01$). At 12 weeks, the NCSC + ES and autograft groups had significantly higher GMI than ES and control groups ($p < 0.05$), but not the NCSC group ($p > 0.05$). Data presented as Mean ± SEM. $^{**}p < 0.01$, $^{*}p < 0.05$.

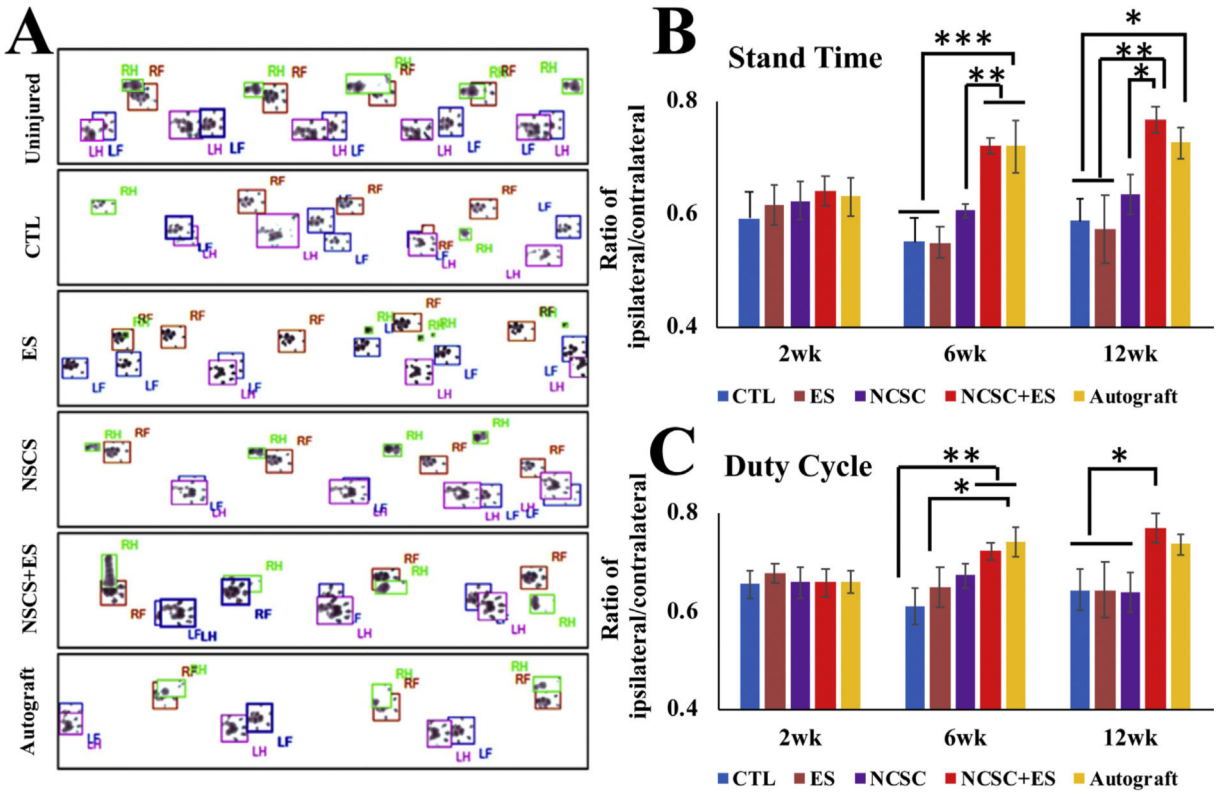

Fig. 8.

(A) representative footprints measured by the Catwalk system after 12 weeks injury, RF = right forepaw, LF = left forepaw, RH = right hindpaw, and LH = left hindpaw. Comparison of locomotion changes between groups over time after nerve repair in (B) *Stand Time* and (C) *Duty Cycle*. Neural crest stem cell (NCSC) + electrical stimulation (ES) showed significant improvements over NCSC, ES, and control groups at 12 weeks for both metrics, and at 6 weeks for stand time (all $p < 0.05$). NCSC + ES showed no significant difference from autograft for both metrics at all time points. Data presented as Mean ± SEM. ***$p \leq 0.001$, **$p \leq 0.01$, *$p \leq 0.05$.